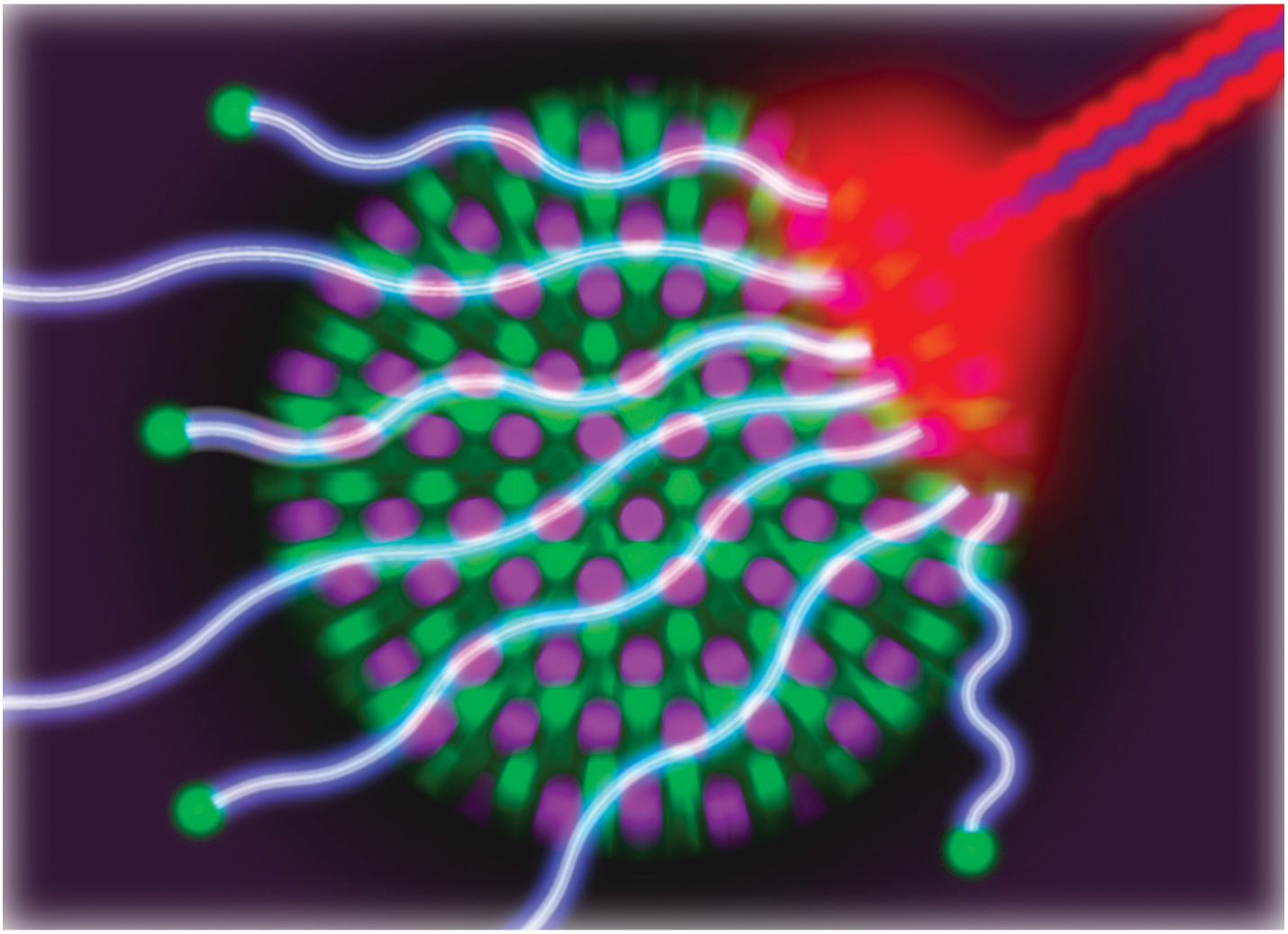

Showcasing research from Bersu Bastug Azer and co-workers, Department of Mechanical and Mechatronics Engineering, University of Waterloo, Ontario, Canada.

Core–shell defective TiO_2 nanoparticles by femtosecond laser irradiation with enhanced photocatalytic performance

Bersu Bastug Azer and co-workers demonstrate a method for creating stable surface defects on TiO_2 nanoparticles using femtosecond laser irradiation. Unlike longer pulse-width lasers such as nanosecond lasers, femtosecond lasers modify only the surface layer, creating core-shell defective TiO_2 while leaving the bulk of the particles intact. This approach increases the photocatalytic performance of TiO_2 by creating active sites and lowering its band gap. These findings hold potential for the development of more efficient and sustainable photocatalytic applications.

As featured in:

See Bersu Bastug Azer, Mustafa Yavuz *et al.*, *Mater. Adv.*, 2023, **4**, 1297.

ROYAL SOCIETY OF CHEMISTRY

rsc.li/materials-advances

Registered charity number: 207890

Materials Advances

ROYAL SOCIETY OF CHEMISTRY

PAPER

View Article Online
View Journal | View Issue

Cite this: *Mater. Adv.*, 2023, 4, 1297

Core–shell defective TiO_2 nanoparticles by femtosecond laser irradiation with enhanced photocatalytic performance†

Bersu Bastug Azer, *[a] Ahmet Gulsaran,[a] Joel R. Pennings,[a] Reza Karimi,[b] Aydin Ashrafi Belgabad,[bc] Alexander H. Xu,[ad] Liena Zaidan,[e] Samed Kocer,[af] Joseph Sanderson,[b] Michal Bajcsy,[eg] Michael A. Pope [ah] and Mustafa Yavuz*[a]

Received 11th January 2023,
Accepted 26th January 2023

DOI: 10.1039/d3ma00019b

rsc.li/materials-advances

Engineering defects in titanium dioxide (TiO_2) is becoming increasingly important to enhance its photocatalytic performance by increasing active sites and lowering its band gap from the UV region to the visible light region. Herein, we demonstrate a simple method to create stable surface defects by exposing TiO_2 dispersions to femtosecond laser irradiation. When using an 800 nm wavelength source, little change to the TiO_2 dispersion is observed. However, including the second harmonic of this source (400 nm wavelength) creates stable, dark colored, defective TiO_2, also known as black TiO_2. This occurs without the formation of a rutile phase, previously thought to be necessary for black TiO_2 formation. We demonstrate that the surface oxygen vacancy concentration can be tuned to a maximum of 8% with irradiation time. Beyond this, defect annihilation is observed. Unlike irradiation using longer pulse width lasers (*e.g.* nanosecond and picosecond lasers), which are known to create more bulk defects, modification using femtosecond pulse widths only modifies a thin shell at the surface, leaving the bulk of the particles unaffected. The most defective TiO_2 exhibits enhanced photocatalytic performance under UV light owing to the formation of defects which act as trapping states for photogenerated electron/hole pairs.

Introduction

TiO_2 is one of the most widely studied materials for various applications since Honda and Fujishima discovered its effective photocatalytic properties.[1] In addition, it is an attractive material because of its low cost, chemical and thermal stabilities, low toxicity, natural abundance, and availability.[2] Consequently, TiO_2 is one of the most prominent materials for photoelectrochemical water splitting,[3,4] dye-sensitized solar cells,[5,6] photoelectrochemical sensors,[7–12] photocatalysis in atmospheric chemistry,[13] photocatalytic degradation of organic pollutants,[14–16] and other photocatalytic applications.[17,18] However, challenges with TiO_2 include its wide band gap energy (3.0–3.2 eV), which restricts light absorption to the high-energy UV region[19] and the typically fast recombination rate of photogenerated electron–hole pairs that reduces device quantum efficiency.[20,21] To overcome these drawbacks, TiO_2 has been modified using different strategies, such as metal doping[22–24] and non-metal doping.[25–28] Despite enhancing the visible light activity of TiO_2, doping enhances electron–hole pair recombination.[29,30] Moreover, it has been reported that doping of TiO_2 also causes secondary phase formation and a decrease in crystallinity, affecting the lifetime of electron–hole pairs.[31]

[a] *Waterloo Institute for Nanotechnology (WIN), University of Waterloo, 200 University Ave. West, Waterloo, ON N2L 3G1, Canada. E-mail: bbastuga@uwaterloo.ca, myavuz@uwaterloo.ca*
[b] *Department of Physics and Astronomy, University of Waterloo, 200 University Ave. West, Waterloo, ON N2L 3G1, Canada*
[c] *Department of Physics and Energy Engineering, Amirkabir University of Technology (Tehran Polytechnic), P.O. Box 15875-4413, Tehran, Iran*
[d] *Department of Nanotechnology Engineering, University of Waterloo, 200 University Ave. West, Waterloo, ON N2L 3G1, Canada*
[e] *Department of Electrical and Computer Engineering, University of Waterloo, 200 University Ave. West, Waterloo, ON N2L 3G1, Canada*
[f] *Department of Systems Design Engineering, University of Waterloo, 200 University Ave. West, Waterloo, ON N2L 3G1, Canada*
[g] *Institute for Quantum Computing, University of Waterloo, 200 University Ave. West, Waterloo, ON N2L 3G1, Canada*
[h] *Department of Chemical Engineering, University of Waterloo, 200 University Ave. West, Waterloo, ON N2L 3G1, Canada*

† Electronic supplementary information (ESI) available: The spectrum of the BBO crystal before and after the application of femtosecond laser. The O1s XPS spectra of untreated TiO_2, TiO_2-15, TiO_2-30, TiO_2-60, TiO_2-90 and TiO_2-120 samples. The VB XPS spectra of untreated TiO_2, TiO_2-15, TiO_2-30, TiO_2-60, TiO_2-90 and TiO_2-120 samples. See DOI: https://doi.org/10.1039/d3ma00019b

In 2011, Chen *et al.*[32] produced black-colored TiO_2 by generating disorder in the surface layers through a hydrogenation process. Since then, the so-called black TiO_2 has become attractive for various applications such as photocatalytic dye degradation,[33] photoelectrochemical applications,[34] photocatalytic water splitting,[35] the development of dye-sensitized solar cells,[36] and Li-ion batteries.[37] The black or other coloration of TiO_2 results from at least one type of defect in the structure, such as the presence of Ti^{3+} species, oxygen vacancies, Ti–H bonds, surface hydroxyl groups (Ti-OH groups), and structural disorder at the surface such as the formation of Ti^{3+} and Ti_2O_3, at the outermost layer.[38] The formation of these defects enhances solar absorption along with the electrical, optical, and photocatalytic properties. Enhanced quantum efficiency of black TiO_2 thought to be caused by the reduced recombination rate of photogenerated charge carriers has also been reported.[39]

Black TiO_2 has been synthesized by various techniques,[38] such as hydrogenation,[32,40] plasma treatment,[41] chemical reduction,[42] and electrochemical reduction.[43] However, these techniques require either high-temperature, high-pressure reactions, or even toxic chemicals.[44] A green and environmentally friendly synthesis technique is needed for black TiO_2 production. Recently, pulsed laser irradiation techniques have been used as a method of nanomaterials synthesis to obtain metals, metal oxides, core–shell structures of metal oxides, and doped oxides.[45] In particular, femtosecond laser pulses have been effectively used to either generate new nanostructures,[46,47] or modify the physical and chemical properties of existing nanoparticles.[48] For example, the pulse laser ablation of a Ti target in liquids has been used to produce TiO_2 with various properties and defect densities.[49,50] By using TiO_2 nanoparticles, laser irradiation in liquids was used to produce disorder on the surface of TiO_2. Russo *et al.*[51] studied the effects of femtosecond laser (800 nm, 35 fs, 1 kHz) irradiation of P25 powders in water. They reported a color change, but they observed that with an increase in the irradiation time, the blue color decreased. In addition to this, they reported a phase transformation from anatase to rutile and then back to anatase with an increase in the laser irradiation time. Chen *et al.*[52] prepared black TiO_2 nanospheres by irradiating third harmonic pulses of a nanosecond Nd:YAG laser (355 nm, 8 ns, 10 Hz), which exhibited good photocatalytic performance under visible light. Zuniga-Ibarra *et al.*[53] used second harmonic pulses of a nanosecond Nd:YAG laser (532 nm, 10 ns, 10 Hz) to synthesize black TiO_2 nanoparticles using pulsed laser irradiation in liquid dispersions. They reported an enhancement in visible light absorption by decreasing the band gap energy from 2.98 eV to 1.84 eV. Lau *et al.*[54] explained how surface and bulk defects were generated by laser irradiation by comparing the ns-355 nm laser and the ps-532 nm laser. They obtained more than 2-fold enhancement in the photoelectrochemical activity of ps-532 nm laser irradiated TiO_2 nanoparticles, even without observing any color change. They explained the color difference between these two samples with the location of defects. Black samples were obtained by irradiating with ns-355 nm and generated mainly bulk defects, while white samples were produced by processing with ps-532 nm laser which created more surface defects. All these studies[52–54] state that the color change is linked to rutile phase formation, which is observed with high pulse width lasers (nanosecond lasers) because of high thermal loads causing bulk defects.

In this work, we study the use of femtosecond laser pulsed irradiation to obtain defective TiO_2 using both the fundamental (800 nm) and the second harmonic (400 nm) pulses from a Ti:sapphire laser with a 1 kHz repetition rate and a pulse duration of 35 fs. For the first time, we observe a color change without rutile phase formation suggesting a novel defect formation mechanism related to the wavelength used and the femtosecond pulse duration. We systematically study the structure and optical properties of the TiO_2 produced and determine that, through this approach, defects are localized to the surface while the bulk of the material remains unchanged. The degradation of the methylene blue dye is used to demonstrate the improved photocatalytic performance of the modified TiO_2.

Experimental

Synthesis of blue TiO_2 by laser irradiation

20 mg of pure TiO_2 (Sigma Aldrich, anatase <25 nm) were added to 1 mL of ultra-pure de-ionized (DI) water and ultrasonicated for 30 minutes. Then, it was irradiated with a combination of fundamental (800 nm) and second harmonic generated pulses ($\lambda = 400$ nm) of a Ti:sapphire pulsed laser with a pulse duration of 35 fs and a repetition rate of 1 kHz. The spectra of the laser before and after barium borate (BBO) non-linear crystal are shown in Fig. S1 (ESI†). The irradiation was performed by constantly mixing the solution with a magnetic stirrer to obtain a homogeneous and uniform solution. A focus lens with a 50 mm focal length was used to focus the beam at a depth of 2 mm inside the solution. The solution was irradiated with average powers of 1 W and 0.8 W at an 800 nm wavelength and 0.2 W at a 400 nm wavelength. The laser fluences of 800 and 400 nm wavelength outputs were estimated as 4074 J cm^{-2} and 1018 J cm^{-2}, respectively. The total laser irradiation time is n minutes. The laser setup is shown in Fig. 1.

After laser irradiation, the samples were left under vacuum to dry at ambient temperature. The prepared samples are indicated as TiO_2-n, where n is the laser irradiation duration in minutes, n = 15, 30, 60, 90, and 120.

Characterization

Powder X-ray diffraction (XRD) was carried out using a Bruker D8-Focus with Cu-Kα radiation at a wavelength of 1.5406 Å, an acceleration voltage of 40 kV, and an emission current of 40 mA.

Ultraviolet/visible (UV-Vis) diffuse reflectance spectroscopy was carried out using a Shimadzu UV-2501PC spectrometer. The absorbance was calculated from the diffuse reflectance values using eqn (1).

$$A = \log\left(\frac{1}{R}\right) \quad (1)$$

where A is the absorbance and R is the diffuse reflectance value obtained from diffuse reflectance. The band gap energies were

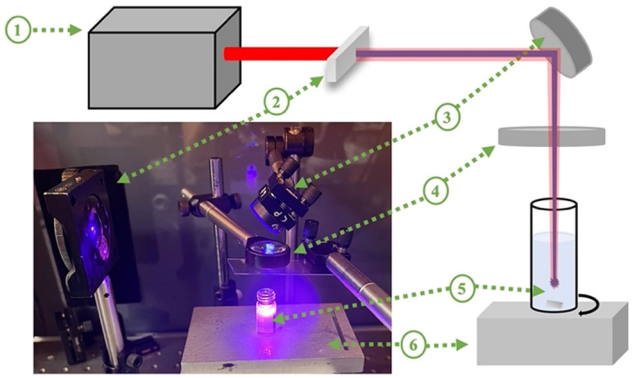

Fig. 1 Schematic representation and photograph of the laser irradiation experiment setup containing the (1) Ti:sapphire pulsed laser, (2) barium borate (BBO) non-linear crystal, (3) mirror, (4) focus lens (f = 50 mm), (5) TiO_2 dispersion with a magnetic stir bar, and (6) magnetic stirrer.

estimated by transforming the data using the Kubelka–Munk function method using eqn (2).

$$F(R) = \frac{(1-R)^2}{2R} \quad (2)$$

The Raman spectra were collected using a Horiba Jobin–Yvon HR800 Raman spectrometer with an Olympus BX 41 microscope. The Raman spectra analyses were carried out using OriginPro 2021b, and peaks were fit with a Gaussian line shape. The excitation wavelength and power were set to 532 nm and 50 mW, respectively.

The chemical states of the samples and the valence band (VB) were identified by X-ray photoelectron spectroscopy (XPS) using a Thermo ESCALAB 25 using an Al-Kα X-ray source. XPS analyses were performed using OriginPro 2021b and Shirley XPS baseline, and Gaussian fitting was performed. The oxygen vacancy content can be calculated from XPS analyses using eqn (3).

$$V_O = \frac{\left[\frac{S_{Ti^{3+}}}{(S_{Ti^{3+}} + S_{Ti^{4+}})}\right]}{4} \times 100\% \quad (3)$$

The morphology of the laser irradiated nanoparticles was examined by scanning electron microscopy (SEM, JEOL JSM-7200F) at an acceleration voltage of 15 kV. Elemental analyses of the bulk structure of untreated and laser treated TiO_2 were performed using an energy dispersive X-ray spectroscopy (EDS, Oxford X-max) detector installed on a SEM.

Photocatalytic reaction

The photocatalytic activity of laser irradiated samples was measured by methylene blue (MB) photodegradation. For a typical reaction, 5 mg of photocatalytic powder was added to 15 mL of a 5 mg L^{-1} concentration of MB solution. Before starting the reaction, the solution was stirred using a magnetic stirrer in the dark for 1 h to establish the equilibrium absorption of MB. Then, the solution was exposed to UV light (Analytik Jena) with a 6 W power with a center wavelength of 365 nm. The pH of suspensions was stable at 7 ± 0.1, the temperature was maintained at 25 ± 1 °C and they were stirred at 400 rpm. Samples with a volume of 2 mL were collected at designated time intervals and centrifuged at 3000 rpm for 20 minutes to remove the dispersed TiO_2 particles. The concentration of MB was obtained by recording the absorbance spectra of the solution in the range of 200–800 nm using a UV-Vis spectrometer with a quartz cuvette. The change in the absorption of MB solution at a 664 nm wavelength during the photodegradation process was monitored. The Lambert–Beer law was used to correlate the absorption to the MB concentration using eqn (4).

$$A = \varepsilon c l \quad (4)$$

where A is the absorbance, ε is the molar absorption coefficient (M^{-1} cm^{-1}), l is the optical path length (cm), and c is the molar concentration (M).

Results and discussion

Morphological and structural properties of TiO_2 nanoparticles

In previous studies,[52–54] it has been suggested that a color change cannot be observed with irradiation of lasers with shorter than nanosecond pulse widths (<ns) because the color change is associated with rutile phase formation. In this study, the stable color change was not observed when pulses of pure 800 nm wavelength radiation were used similar to the study of Russo *et al.*[51] They reported that the increase in the ablation time resulted in a less blue colour intensity, but they did not mention the stability of the blue TiO_2 samples. In this study, when the 800 nm wavelength output was used, samples were observed to turn blue, but returned to a white on the time scale of minutes. On the other hand, after generating the second harmonic (400 nm) using a BBO crystal and combining it with the fundamental (800 nm) light, a significant and stable color change was observed without any rutile phase formation, as shown in Fig. 2b. The effect of the laser wavelength on the defect formation mechanism has not been fully explained in the literature yet. We did not observe any stable color and structural change with laser irradiation at an 800 nm wavelength. However, when we created the second harmonic, the combination of 800 nm and 400 nm wavelengths resulted in the defect formation. We also attempted to filter out the 800 nm wavelength and ablate TiO_2 solution with only a 400 nm wavelength to understand the effect of each wavelength well.

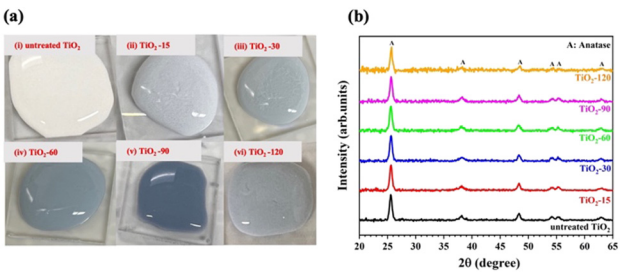

Fig. 2 (a) Photographs of TiO_2 dispersions obtained before and after laser irradiation: (i) untreated TiO_2, (ii) TiO_2-15, (iii) TiO_2-30, (iv) TiO_2-60, (v) TiO_2-90 and (vi) TiO_2-120 and (b) XRD analysis of TiO_2 samples before and after laser irradiation.

However, this reduced the intensity of the 400 nm light significantly. This yielded no observable change either due to the low power or due to the absence of the 800 nm wavelength.

As shown in Fig. 2a, the color of the TiO_2 dispersions changed from white to blue-gray upon laser irradiation for a 15 minute duration. Further increasing the laser irradiation time darkened the coloration, reaching a maximum darkness after 90 minutes. However, extending the irradiation time further, to 120 minutes, resulted in a lighter colored dispersion. The color of the samples suggests that they can absorb visible light partially or totally.

The crystalline structure of samples before and after laser irradiation was studied by XRD analysis. Laser irradiation did not affect the phases present in the structure, as shown in Fig. 2b. The XRD patterns of all samples are composed of diffraction peaks at 25.2, 36.9, 37.7, 38.5, 47.9, 53.8, 54.9, 61.9, and 62.5 degrees, corresponding to the (101), (103), (004), (112), (200), (105), (211), (213) and (204) lattice planes of the anatase phase of TiO_2 (JCPDS Card No. 21-1272).

This result is new for femtosecond irradiated TiO_2 as previously only nanosecond irradiation was able to induce a color change.[45,54] In the previous ns irradiation works, the observed color change has always been associated with rutile phase formation. The authors argued that this phase transformation occurs *via* recrystallization after isochoric melting occurs. On the other hand, lower energy but focused femtosecond laser pulses can cause ablative surface ionization.[45] Light–matter interactions with femtosecond lasers are usually athermal and thus melting and the associated recrystallization process cannot occur. Only defect formation occurs, and these defects are localized at the surface due to surface ionization. Here, we have shown that not only the pulse width but also the wavelength plays a role in the color change mechanism induced by femtosecond laser irradiation. One possible explanation for this could be the introduction of photoinduced defects through the introduction of electron/hole pairs generated by the single photon absorption of 400 nm radiation as follows:

$$TiO_2 + h\nu \rightarrow e_{CB}^- + h_{VB}^+ \quad (5)$$

The electrons tend to reduce Ti^{4+} cations to the Ti^{3+} state as shown in eqn (6),

$$e_{CB}^- + Ti^{4+} + Ti^{3+} \quad (6)$$

and holes oxidize O^{2-} anions to form O^- as in eqn (7),

$$h_{VB}^+ + O^{2-} \rightarrow O^- \quad (7)$$

Ti^{3+}/oxygen vacancy pairs are obtained after exciting electron/hole pairs with enough photon energy, as given in eqn (6) and (7). It has been suggested by many that an optically active defect family exists in the energy range of 390–510 nm, in agreement with previous studies.[54–56] Since 800 nm is not in this range, it is, therefore, unable to excite electron/hole pairs to create optically active defects. This can also explain the unstable color change when only 800 nm radiation is used. On the other hand, the 400 nm light falls within this range and is able to generate electron/hole pairs resulting in optically active defects.

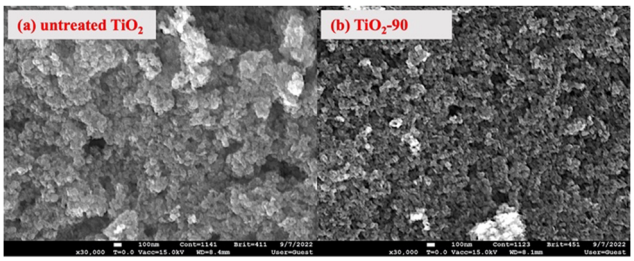

Fig. 3 SEM micrographs of TiO_2 before and after laser irradiation: (a) untreated TiO_2 and (b) TiO_2-90.

The morphological analyses of nanoparticles before and after laser irradiation were performed by scanning electron microscopy (SEM), as shown in Fig. 3. As seen from the SEM images, there was no significant morphological change after laser irradiation. It was also seen that the femtosecond laser irradiation does not impact the particle size. There are some agglomerates and nanoparticles in the structure before and after laser irradiation. This behavior does not match with nanosecond laser irradiated TiO_2 as well. Chen *et al.*[52] reported that as the laser irradiation time increased, the particle size decreased. Similarly, Zuñiga-Ibarra *et al.*[53] showed a morphological change with laser irradiation, and they demonstrated an increased number of agglomerates and small nanoparticles with an increase in the laser irradiation time. They explained this behavior by applying enough energy to melt TiO_2 and the nucleation and growth of modified TiO_2 nanoparticles, which is also explained by rutile phase formation. In this study, no morphological and crystallinity changes were observed, and this can be concluded that femtosecond laser might only form defects on the surface of nanoparticles without melting TiO_2, leading to the nucleation and growth of modified nanoparticles.

Raman spectroscopy was performed to determine the crystallinity and molecular interactions of untreated and laser irradiated samples. The spectra shown in Fig. 4a show peaks at the major Raman bands at around 143 cm^{-1}, 197 cm^{-1}, 396 cm^{-1}, 514 cm^{-1}, and 639 cm^{-1} which correspond to the six Raman active modes of anatase, which are E_g, E_g, B_{1g}, A_{1g}/B_{1g}, and E_g, respectively.[57–59] The strongest peak at around 143 cm^{-1} in the neat sample is caused by symmetric vibrations of oxygen atoms in the O–Ti–O bond. The position of this peak shifts positively, increasing to 147.3 cm^{-1} for TiO_2-90 and then decreasing with further treatment time to 120 minutes, as shown in Fig. 4b. The intensity of the peak decreased and broadened. This suggests that the O–Ti–O bond amount decreased in the structure by increasing the laser irradiation time up to 90 minutes. After 90 minutes, the peak intensity increased, the peak narrowed, and a negative shift was observed from TiO_2-90. The full-width-at-half-maximum (FWHM) values were calculated for each sample by the Gaussian fitting curve, as shown in Fig. 4c.

Raman spectroscopy is an effective tool for determining the surface oxygen vacancies on the structure.[60] It was reported that the broadening of A_{1g}/B_{1g} mode by a FWHM value of 0.25 cm^{-1} corresponds to the increment of 1% oxygen vacancy in the lattice structure.[61] A_{1g}/B_{1g} peaks were Gaussian fitted, and the

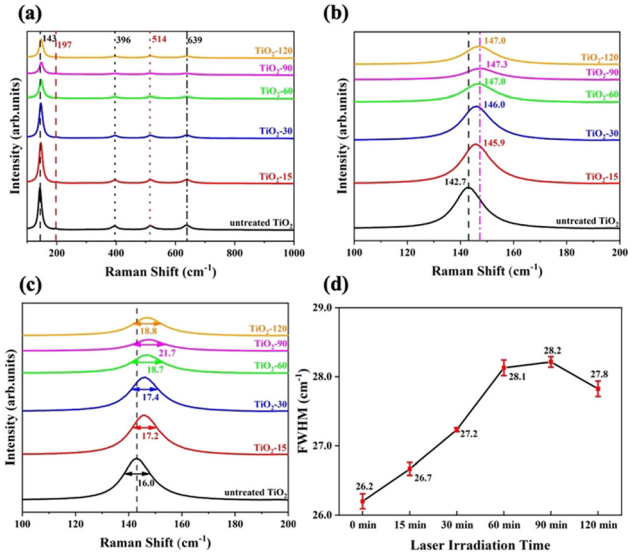

Fig. 4 Raman spectra of TiO_2 before and after laser irradiation: (a) spectra with peak values, (b) the peak position of the strongest Raman peak, (c) the enlarged strongest Raman peak, and (d) FWHM values from the Gaussian fitted A_{1g}/B_{1g} peak of untreated TiO_2, TiO_2-15, TiO_2-30, TiO_2-60, TiO_2-90, and TiO_2-120. The units of peak values are cm^{-1}.

FWHM values were calculated for untreated and laser irradiated samples, as shown in Fig. 4d. The data indicate that TiO_2-90 has the highest amount of oxygen vacancies, which is 8% more than untreated TiO_2. The oxygen vacancy concentration of TiO_2-15 was estimated to be 2% more than untreated TiO_2, the oxygen vacancy of TiO_2-30 was 4% more than untreated TiO_2, TiO_2-60 had 7.6% more oxygen vacancy than untreated TiO_2, and the oxygen vacancy of TiO_2-120 was 6.4% more than untreated TiO_2. This showed that increasing the laser irradiation time after 90 minutes led to a decrease in the oxygen vacancy content. By femtosecond laser irradiation, oxygen atoms were removed from the TiO_2 surface because of localized heating. With an increase in the laser irradiation time from 90 to 120 minutes, further oxygen removal could not occur, and oxygen atoms were bonded with Ti to form Ti^{4+}–O, resulting in a decrease in the oxygen vacancy concentration.

Optical properties of TiO_2 nanoparticles

The UV-Vis diffuse reflectance spectra of the various samples are shown in Fig. 5a while Fig. 5b shows absorbance spectra. After laser irradiation, all laser irradiated TiO_2 samples exhibit absorption throughout the visible light region when compared with untreated TiO_2. Furthermore, the absorption of visible light above the 400 nm wavelength increased as the laser irradiation time increased up to 90 minutes.

The band gap energies of untreated and laser irradiated TiO_2 nanomaterials are evaluated by the Kubelka–Munk function method using eqn (2). The determined band gap energy values are shown in Fig. 5c. The band gap energy of TiO_2 shifts from 3.2 eV to 2.9 eV by laser irradiation for 90 minutes. The oxygen vacancies and other defects might have created additional energy levels between the valence band (VB) and the conduction band (CB) of TiO_2. TiO_2-90 has 8% more oxygen vacancies than untreated TiO_2, and the band gap energy of TiO_2-90 decreased from 3.2 eV to 2.9 eV. This supports the previous studies that reported oxygen vacancies to cause enhanced visible light absorption below the direct band gap.[29,52]

The lowest band gap energy obtained from laser irradiated samples is 2.9 eV. After increasing the laser irradiation time from 90 to 120 minutes, the band gap energy increased from 2.9 eV to 3 eV. This also matches the oxygen vacancy concentration obtained from the FWHM values of A_{1g}/B_{1g} mode, as shown in Fig. 4d. The oxygen vacancy of TiO_2-90 is 0.4% more than that of TiO_2-120.

Chemical state analysis of TiO_2 nanoparticles

XPS analysis was carried out to determine the change of surface chemical constituents caused by laser irradiation. The surface of the samples is clean from impurities except for a trace amount of C. Ti, O, and C elements were found from the survey scan (Fig. 6a). The Ti 2p XPS spectra of untreated TiO_2, TiO_2-15, TiO_2-30, TiO_2-60, TiO_2-90 and TiO_2-120 are shown in Fig. 6b. The energy and area of each peak for every sample are given in Table 1. The peaks at 459.7 eV and 465.4 eV are Ti^{4+} $2p_{3/2}$ and Ti^{4+} $2p_{1/2}$ XPS peaks, respectively. For laser irradiated samples, two new peaks appeared between 459.3 and 459.5 eV and

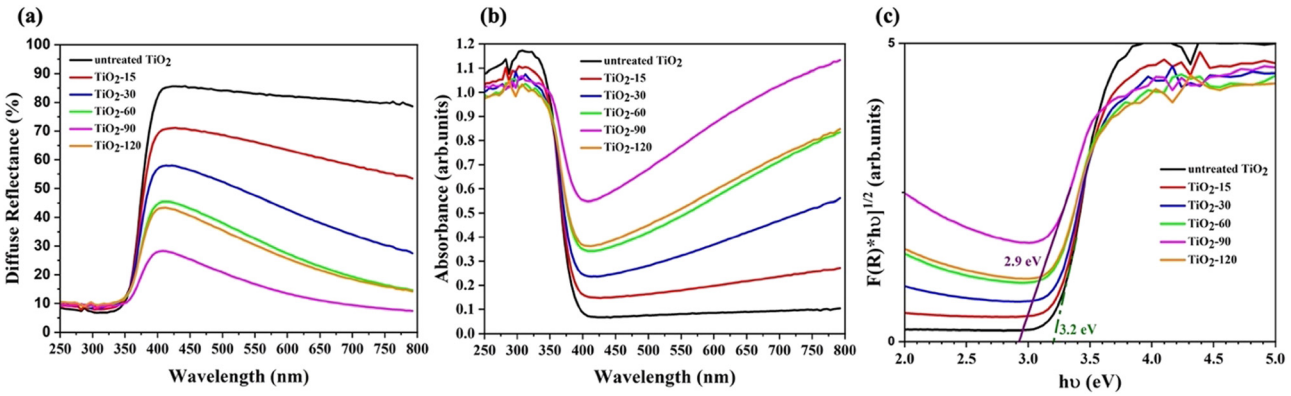

Fig. 5 Optical properties of TiO_2 before and after laser irradiation: (a) UV-Vis diffuse reflectance spectra, (b) absorbance spectra, and (c) $[F(R) \times h\nu]^{1/2}$ *vs.* $h\nu$ curves of untreated and laser irradiated TiO_2.

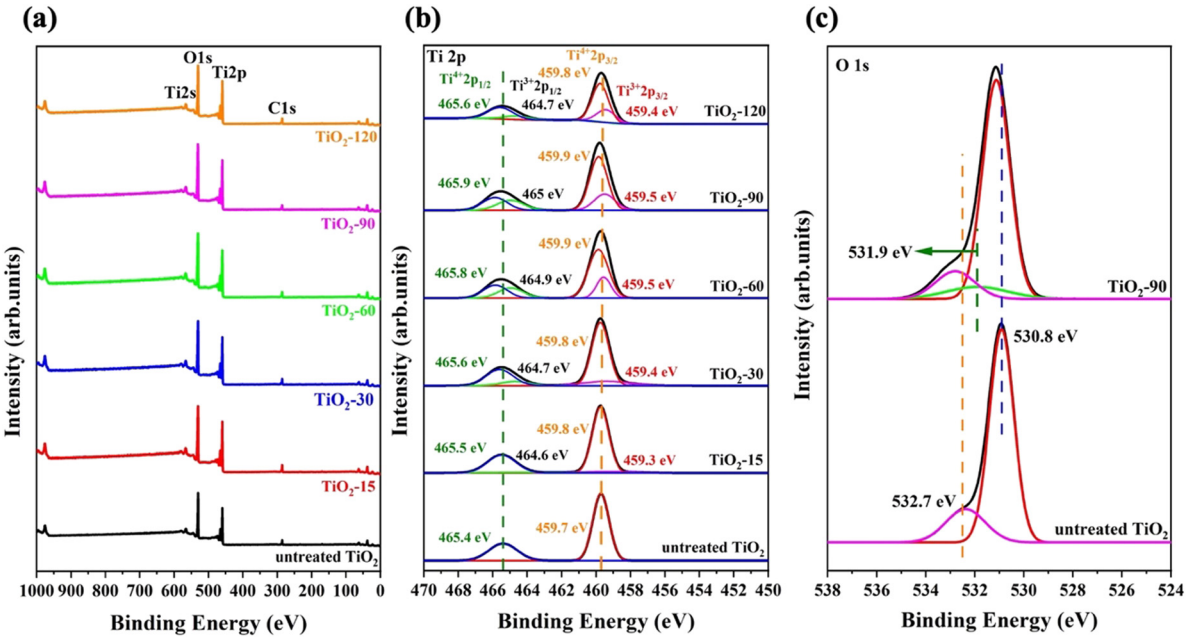

Fig. 6 XPS spectra of TiO_2 before and after laser irradiation: (a) survey, (b) Ti 2p XPS spectra of untreated TiO_2, TiO_2-15, TiO_2-30, TiO_2-60, TiO_2-90 and TiO_2-120, and (c) O 1s XPS spectra of untreated TiO_2 and TiO_2-90.

464.7 and 465 eV, depending on the laser irradiation time, and they are assigned to Ti^{3+} $2p_{3/2}$ and Ti^{3+} $2p_{1/2}$, respectively. The binding energy of Ti^{4+} $2p_{1/2}$ shifted to 0.5 eV for TiO_2-90 compared to that of untreated TiO_2, which is the maximum shift for laser irradiated samples. Similarly, the positive shifts of Ti^{4+} $2p_{3/2}$, Ti^{3+} $2p_{3/2}$, and Ti^{3+} $2p_{1/2}$ were observed, which are probably because of the formation of oxygen vacancies which causes the bond length of Ti–O to shorten, resulting in a positive shift in the XPS peaks.[61]

Eqn (3) was used to calculate the oxygen vacancy content for all laser irradiated samples and the values are provided in Table 2. The oxygen vacancy contents calculated from XPS analysis are consistent with the Raman results.

Fig. 6c shows the XPS O 1s peaks of untreated TiO_2 and TiO_2-90. For untreated TiO_2, two peaks appear, and the one at 530.8 eV is assigned to the lattice oxygen of TiO_2 because of the Ti^{4+}–O bond, while the peak at 532.7 eV is attributed to adsorbed oxygen. For TiO_2-90, these peaks show positive peaks by 0.2 eV and 0.1 eV to 531 eV and 532.8 eV, respectively. In addition, a new peak also appears at 531.9 eV and corresponds to hydroxyl oxygen (Ti–OH). The O 1s XPS spectra of TiO_2-15, TiO_2-30, TiO_2-60, and TiO_2-120 are given in Fig. S2 in the ESI.†

Table 2 Oxygen vacancy contents of laser irradiated samples using eqn (3)

Samples	V_O
Untreated TiO_2	—
TiO_2-15	1.99%
TiO_2-30	4.27%
TiO_2-60	7.57%
TiO_2-90	8.05%
TiO_2-120	6.58%

The elemental composition of the bulk structure of untreated and laser modified TiO_2 was determined by EDS analysis. Ti, O, and C elements were found in the samples. The atomic percentages of each element for all samples are given in Table 3. The O/Ti ratio of all samples is close to 2 with no systematic variations. This suggests that significant oxygen vacancies are not introduced into the bulk of the material since it is known that the EDS analysis gives information about the bulk of the sample of the large interaction volume of high energy electrons which produce the X-rays generated. Since the XPS and Raman spectra

Table 1 Peak energies and peak areas of Ti 2p XPS analysis of untreated TiO_2, TiO_2-15, TiO_2-30, TiO_2-60, TiO_2-90 and TiO_2-120

	Ti^{4+} $2p_{1/2}$		Ti^{3+} $2p_{1/2}$		Ti^{4+} $2p_{3/2}$		Ti^{3+} $2p_{3/2}$	
Sample	Peak energy (eV)	Peak area	Peak energy (eV)	Peak area	Peak energy (eV)	Peak area	Peak energy (eV)	Peak area
Untreated TiO_2	465.4	21433.74	—	—	459.7	49213.07	—	—
TiO_2-15	465.5	14563.02	464.6	1473.82	459.8	31530.21	459.3	2511.86
TiO_2-30	465.6	12297.05	464.7	3244.98	459.8	30809.21	459.4	5635.04
TiO_2-60	465.8	10653.7	464.9	8783.12	459.9	33499.92	459.5	10379.01
TiO_2-90	465.9	11736.76	465	9820.84	459.9	35794.13	459.5	12735.9
TiO_2-120	465.6	19588.54	464.7	6004.09	459.8	42541.09	459.4	16197.21

Table 3 EDS analysis of untreated TiO_2, TiO_2-15, TiO_2-30, TiO_2-60, TiO_2-90 and TiO_2-120. The units are atomic%

Sample	Ti (at%)	O (at%)	C (at%)	O/Ti ratio
Untreated TiO_2	32.15	62.71	5.14	1.95
TiO_2-15	32.35	62.55	5.1	1.93
TiO_2-30	32.11	62.86	5.03	1.96
TiO_2-60	31.91	62.97	5.12	1.97
TiO_2-90	32.31	63.11	4.58	1.95
TiO_2-120	32.05	62.87	5.08	1.96

are surface sensitive and EDS is not, the laser treated samples have a defective shell with an unmodified core, and core–shell defective TiO_2 has been produced.

The high-resolution VB XPS spectra of untreated TiO_2 and TiO_2-90 are given in Fig. 7a. The VB maximum values of untreated TiO_2 and TiO_2-90 are 3.49 eV and 3.74 eV, which shows a 0.4 eV shift of the maximum value above by the laser irradiation of TiO_2. The VB XPS spectra of TiO_2-15, TiO_2-30, TiO_2-60, and TiO_2-120 are given in Fig. S3 in the ESI.†

The band gap energies obtained from the Kubelka–Munk function from the UV-Vis diffuse reflectance measurement (Fig. 5c) suggest a downward shift of the CB minimum of 0.025 eV. With this information, a schematic illustration of the band structure of untreated TiO_2 before and after femtosecond laser modification is shown in Fig. 7b. The formation of Ti^{3+} species, oxygen vacancies, Ti–OH bonds, and surface disorder caused by femtosecond laser irradiation are probably for band tail states around the VB maximum and the CB minimum.

Photocatalytic performance of TiO_2 nanoparticles

Many researchers have identified that surface and bulk defects, *i.e.*, Ti^{3+} and oxygen vacancies, can improve the photocatalytic performance of TiO_2 by narrowing the band gap and providing more catalytic adsorption sites. However, surface defects are more efficient at trapping and separating photogenerated electron–hole pairs, whereas bulk defects can act as recombination centers for such photogenerated charge carriers.[62–64] The Raman and XPS spectra show the oxygen vacancies and Ti^{3+} species formation on the surface, suggesting that laser modified TiO_2 can potentially exhibit better photocatalytic performance. To test this, the breakdown of the MB dye was compared with untreated TiO_2 and TiO_2-90 as the photocatalytic materials. TiO_2-90 was chosen to compare with untreated TiO_2 since it has the most oxygen vacancies according to the Raman and XPS results. The untreated TiO_2 and TiO_2-90 were mixed with MB, and the degradation of MB was measured under ultraviolet light by recording the C/C_0 ratio, as shown in Fig. 8. A decrease in the MB concentration was observed with the increasing ultraviolet light exposure time. It was also found that when no light was used, the decrease in the concentration was insignificant, indicating that only the photocatalytic process was responsible for the decrease. The degradation rates of MB were 80% for TiO_2-90 and 50% for untreated TiO_2 after exposure to ultraviolet light for 3 hours.

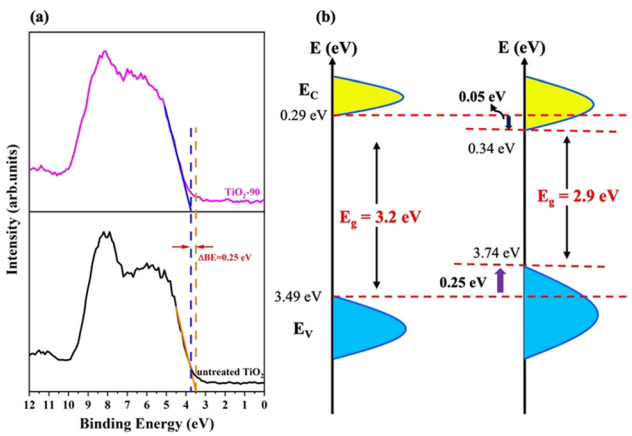

Fig. 7 (a) High-resolution valence band XPS spectra and (b) schematic illustration of the electronic density of states of untreated TiO_2 and TiO_2-90.

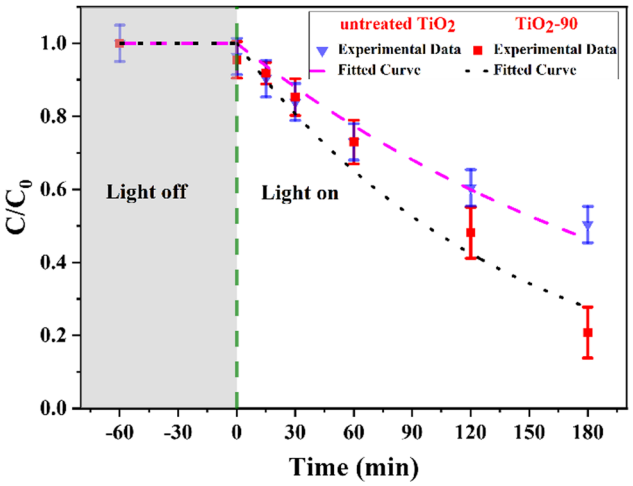

Fig. 8 Photocatalytic degradation of methylene blue under UV light irradiation of untreated TiO_2 and TiO_2-90.

During the femtosecond laser irradiation process, oxygen vacancies were formed on the surface. To maintain the charge neutrality, some of the Ti^{4+} were transformed to Ti^{3+}. Since the reaction occurred in an aqueous environment, some Ti^{3+} species tended to bond with H_2O and resulted in the formation of surface functional groups such as Ti–OH as obtained from the XPS analysis. Oxygen vacancies, Ti^{3+}, Ti–OH, and general surface disorder might act as trapping centers by locally shifting energy levels below the CB and above the VB, and they can reduce the recombination rate of photogenerated electron–hole pairs.[65] It was stated that oxygen vacancies acted as electron donors and contributed to the increased donor density.[40] This can improve the charge transport and shift the CB and the VB, as shown in this study. These shifts can make electron/hole separation easier, resulting in better photocatalytic activity.[66]

Conclusions

In this study, the combination of fundamental and second harmonic radiations from a femtosecond laser was used to produce core–shell, defective TiO_2. Unlike the literature, a new

defect formation mechanism has been introduced relating the defect generation to the wavelength of the laser. The influence of laser irradiation on the oxygen vacancy concentration and photocatalytic performance was revealed. The femtosecond laser surface irradiation led to the formation of Ti^{3+}, oxygen vacancies, and Ti–OH on the TiO_2 surface without deforming the bulk of the sample. According to the Raman and XPS spectra analyses, a maximum of 8% oxygen vacancies were produced on the surface by femtosecond laser irradiation, which narrowed the band gap energy of TiO_2 from 3.2 eV to 2.9 eV by shifting the VB maximum and CB minimum values. The EDS analysis showed that the bulk of the sample is stoichiometric TiO_2, which suggests that by femtosecond laser irradiation, TiO_2 nanoparticles with an undefective core with a defective shell could be formed. The femtosecond laser modified defective core–shell structured TiO_2 exhibited better photocatalytic performance under ultraviolet light exposure owing to the formation of oxygen vacancies, Ti^{3+} and surface disorders, which might act as trapping centers for photogenerated charge carriers and can result in a reduction in the recombination rate. To further explain the defect formation mechanism, different wavelengths with different pulse width lasers should be used to demonstrate the formation of surface defects and bulk defects in TiO_2 and other metal oxides. Their effect on photocatalytic performance under various light sources should be studied. In the literature, it is known that surface defects positively affect the electronic properties of TiO_2, which suggests that the surface defective TiO_2 can be a promising material for the functionalization of different sensing applications such as biosensing, gas sensing, and electrochemical sensing.

Conflicts of interest

There are no conflicts to declare.

Acknowledgements

This research was funded by the CMC Microsystems, Canadian Mathematics of Information Technology and Complex Systems Agency (MITACS) [Grant No: IT17161 and 2000-2024], the NSERC Alliance [Grant No: ALLRP 554872-20], and the Discovery [Grant No: GPIN-2020-06053] research programs. The University of Waterloo's QNFCF (Quantum-Nano Fabrication and Characterization Facility) facility was used for this work.

Notes and references

1 A. Fujishima and K. Honda, *Nature*, 1972, **238**, 37.
2 K. Nakata and A. Fujishima, *J. Photochem. Photobiol., C*, 2012, **13**, 169.
3 G. Wang, H. Wang, Y. Ling, Y. Tang, X. Yang, R. C. Fitzmorris, C. Wang, J. Z. Zhang and Y. Li, *Nano Lett.*, 2011, **11**, 3026.
4 Z. Yu, H. Liu, M. Zhu, Y. Li and W. Li, *Small*, 2021, **17**, 1903378.
5 Z. Wang, H. Kawauchi, T. Kashima and H. Arakawa, *Coord. Chem. Rev.*, 2004, **248**, 1381.
6 M. S. Ahmad, A. K. Pandey and N. A. Rahim, *Renewable Sustainable Energy Rev.*, 2017, **77**, 89.
7 S. Zhang, S. Zhang, B. Peng, H. Wang, H. Yu, H. Wang and F. Peng, *Electrochem. Commun.*, 2014, **40**, 24.
8 R. Wang, M. Zu, S. Yang, S. Zhang, W. Zhou and Z. Mai, *Sens. Actuators, B*, 2018, **270**, 270.
9 M. Zu, M. Zheng, S. Zhang, C. Xing, M. Zhou, H. Liu, X. Zhou and S. Zhang, *Sens. Actuators, B*, 2020, **321**, 128504.
10 X. Wang, S. Zhang, H. Wang, H. Yu, H. Wang, S. Zhang and F. Peng, *RSC Adv.*, 2015, **5**, 76315.
11 Y. Wang, M. Zu, X. Zhou, H. Lin, F. Peng and S. Zhang, *Chem. Eng. J.*, 2020, **381**, 122605.
12 B. Bastug Azer, A. Gulsaran, J. R. Pennings, R. Saritas, S. Kocer, J. L. Bennett, Y. Devdas Abhang, M. A. Pope, E. Abdel-Rahman and M. Yavuz, *J. Electroanal. Chem.*, 2022, **918**, 116466.
13 H. Chen, C. E. Nanayakkara and V. H. Grassian, *Chem. Rev.*, 2012, **112**, 5919.
14 D. Chen, Y. Cheng, N. Zhou, P. Chen, Y. Wang, K. Li, S. Huo, P. Cheng, P. Peng, R. Zhang, L. Wang, H. Liu, Y. Liu and R. Ruan, *J. Cleaner Prod.*, 2020, **268**, 121725.
15 H. Dong, G. Zeng, L. Tang, C. Fan, C. Zhang, X. He and Y. He, *Water Res.*, 2015, **79**, 128.
16 P. Pascariu, C. Cojocaru, M. Homocianu, P. Samoila, A. Dascalu and M. Suchea, *Ceram. Int.*, 2022, **48**, 4953.
17 K. Nakata and A. Fujishima, *J. Photochem. Photobiol., C*, 2012, **13**, 169.
18 Q. Guo, C. Zhou, Z. Ma and X. Yang, *Adv. Mater.*, 2019, **31**, 1901997.
19 S. G. Ullattil, S. B. Narendranath, S. C. Pillai and P. Periyat, *Chem. Eng. J.*, 2018, **343**, 708.
20 V. Binas, D. Venieri, D. Kotzias and G. Kiriakidis, *J. Materiomics*, 2017, **3**, 3.
21 W. Fang, M. Xing and J. Zhang, *J. Photochem. Photobiol., C*, 2017, **32**, 21.
22 M. Zhang, S. Yuan, Z. Wang, Y. Zhao and L. Shi, *Appl. Catal., B*, 2013, **134**, 185.
23 B. Gao, T. Wang, X. Fan, H. Gong, H. Guo, W. Xia, Y. Feng, X. Huang and J. He, *Inorg. Chem. Front.*, 2017, **4**, 898.
24 M. Pelaez, N. T. Nolan, S. C. Pillai, M. K. Seery, P. Falaras, A. G. Kontos, P. S. M. Dunlop, J. W. J. Hamilton, J. A. Byrne, K. O'Shea, M. H. Entezari and D. D. Dionysiou, *Appl. Catal., B*, 2012, **125**, 331.
25 Y. Chen, A. Li, Q. Li, X. Hou, L. N. Wang and Z. H. Huang, *J. Mater. Sci. Technol.*, 2018, **34**, 955.
26 P. S. Basavarajappa, S. B. Patil, N. Ganganagappa, K. R. Reddy, A. V. Raghu and C. V. Reddy, *Int. J. Hydrogen Energy*, 2020, **45**, 7764.
27 W. Yuan, L. Cheng, Y. An, S. Lv, H. Wu, X. Fan, Y. Zhang, X. Guo and J. Tang, *Adv. Sci.*, 2018, **5**, 1700870.
28 S. B. Patil, P. S. Basavarajappa, N. Ganganagappa, M. S. Jyothi, A. V. Raghu and K. R. Reddy, *Int. J. Hydrogen Energy*, 2019, **44**, 13022.
29 F. Zuo, L. Wang, T. Wu, Z. Zhang, D. Borchardt and P. Feng, *J. Am. Chem. Soc.*, 2010, **132**, 11856.

30 H. U. Lee, S. C. Lee, S. H. Choi, B. Son, S. J. Lee, H. J. Kim and J. Lee, *Appl. Catal., B*, 2013, **129**, 106.
31 S. G. Ullattil and P. Periyat, *J. Mater. Chem. A*, 2016, **4**, 5854.
32 X. Chen, L. Liu, P. Y. Yu and S. S. Mao, *Science*, 2011, **331**, 746.
33 T. Leshuk, R. Parviz, P. Everett, H. Krishnakumar, R. A. Varin and F. Gu, *ACS Appl. Mater. Interfaces*, 2013, **5**, 1892.
34 H. Cui, W. Zhao, C. Yang, H. Yin, T. Lin, Y. Shan, Y. Xie, H. Gu and F. Huang, *J. Mater. Chem. A*, 2014, **2**, 8612.
35 B. Wang, S. Shen and S. S. Mao, *J. Materiomics*, 2017, **3**, 96.
36 S. G. Ullattil, A. V. Thelappurath, S. N. Tadka, J. Kavil, B. K. Vijayan and P. Periyat, *Sol. Energy*, 2017, **155**, 490.
37 Y. Yan, B. Hao, D. Wang, G. Chen, E. Markweg, A. Albrecht and P. Schaaf, *J. Mater. Chem. A*, 2013, **1**, 14507.
38 S. G. Ullattil, S. B. Narendranath, S. C. Pillai and P. Periyat, *Chem. Eng. J.*, 2018, **343**, 708.
39 T. S. Rajaraman, S. P. Parikh and V. G. Gandhi, *Chem. Eng. J.*, 2020, **389**, 123918.
40 A. Naldoni, M. Allieta, S. Santangelo, M. Marelli, F. Fabbri, S. Cappelli, C. L. Bianchi, R. Psaro and V. Dal Santo, *J. Am. Chem. Soc.*, 2012, **134**, 7600.
41 Z. Wang, C. Yang, T. Lin, H. Yin, P. Chen, D. Wan, F. Xu, F. Huang, J. Lin, X. Xie and M. Jiang, *Adv. Funct. Mater.*, 2013, **23**, 5444.
42 Q. Kang, J. Cao, Y. Zhang, L. Liu, H. Xu and J. Ye, *J. Mater. Chem. A*, 2013, **1**, 5766.
43 H. Zhou and Y. Zhang, *J. Phys. Chem. C*, 2014, **118**, 5626.
44 X. Chen, L. Liu and F. Huang, *Chem. Soc. Rev.*, 2015, **44**, 1861.
45 V. Amendola, D. Amans, Y. Ishikawa, N. Koshizaki, S. Scirè, G. Compagnini, S. Reichenberger and S. Barcikowski, *Chem. – Eur. J.*, 2020, **26**, 9206.
46 K. Ibrahim, I. Novodchuk, K. Mistry, M. Singh, C. Ling, J. Sanderson, M. Bajcsy, M. Yavuz and K. P. Musselman, *Small*, 2019, **15**, 1904415.
47 Y. Taguchi, H. Endo, T. Kodama, Y. Achiba, H. Shiromaru, T. Wakabayashi, B. Wales and J. H. Sanderson, *Carbon*, 2017, **115**, 169.
48 I. Novodchuk, M. Kayaharman, K. Ibrahim, S. Al-Tuairqi, M. Irannejad, E. Abdel-Rahman, J. Sanderson, M. Bajcsy and M. Yavuz, *Carbon*, 2020, **158**, 624.
49 A. Singh, J. Vihinen, E. Frankberg, L. Hyvärinen, M. Honkanen and E. Levänen, *Nanoscale Res. Lett.*, 2016, **11**, 1.
50 A. S. Nikolov, P. A. Atanasov, D. R. Milev, T. R. Stoyanchov, A. D. Deleva and Z. Y. Peshev, *Appl. Surf. Sci.*, 2009, **255**, 5351.
51 P. Russo, R. Liang, R. X. He and Y. N. Zhou, *Nanoscale*, 2017, **9**, 6167.
52 X. Chen, D. Zhao, K. Liu, C. Wang, L. Liu, B. Li, Z. Zhang and D. Shen, *ACS Appl. Mater. Interfaces*, 2015, **7**, 16070.
53 V. A. Zuñiga-Ibarra, S. Shaji, B. Krishnan, J. Johny, S. Sharma Kanakkillam, D. A. Avellaneda, J. A. A. Martinez, T. K. D. Roy and N. A. Ramos-Delgado, *Appl. Surf. Sci.*, 2019, **483**, 156.
54 M. Lau, S. Reichenberger, I. Haxhiaj, S. Barcikowski, A. M. Müller and A. C. S. Appl, *Energy Mater.*, 2018, **1**, 5366.
55 J. Yan, G. Wu, N. Guan, L. Li, Z. Li and X. Cao, *Phys. Chem. Chem. Phys.*, 2013, **15**, 10978.
56 A. K. Kunti, K. C. Sekhar, M. Pereira, M. J. M. Gomes and S. K. Sharma, *AIP Adv.*, 2017, **7**, 015021.
57 H. Berger, H. Tang and F. Lévy, *J. Cryst. Growth*, 1993, **130**, 108.
58 T. Sekiya, S. Ohta, S. Kamei, M. Hanakawa and S. Kurita, *J. Phys. Chem. Solids*, 2001, **62**, 717.
59 H. C. Choi, Y. M. Jung and S. B. Kim, *Vib. Spectrosc.*, 2005, **37**, 33.
60 Q. Liu, F. Wang, H. Lin, Y. Xie, N. Tong, J. Lin, X. Zhang, Z. Zhang and X. Wang, *Catal. Sci. Technol.*, 2018, **8**, 4399.
61 X. Bi, G. Du, A. Kalam, D. Sun, Y. Yu, Q. Su, B. Xu and A. G. Al-Sehemi, *Chem. Eng. Sci.*, 2021, **234**, 116440.
62 L. Hou, Z. Guan, T. Liu, C. He, Q. Li and J. Yang, *Int. J. Hydrogen Energy*, 2019, **44**, 8109.
63 X. Xing, M. Zhang, L. Hou, L. Xiao, Q. Li and J. Yang, *Int. J. Hydrogen Energy*, 2017, **42**, 28434.
64 M. Kong, Y. Li, X. Chen, T. Tian, P. Fang, F. Zheng and X. Zhao, *J. Am. Chem. Soc.*, 2011, **133**, 16414.
65 Y. Zou, K. Yang, Q. Chen, H. Wang and X. Meng, *RSC Adv.*, 2018, **8**, 36819.
66 H. Tan, Z. Zhao, M. Niu, C. Mao, D. Cao, D. Cheng, P. Feng and Z. Sun, *Nanoscale*, 2014, **6**, 10216.